REPORT ON PROGRESS

Charge density waves in strongly correlated electron systems

IOP Publishing Reports on Progress in Physics
Rep. Prog. Phys. **79** (2016) 084505 (15pp) doi:10.1088/0034-4885/79/8/084505

Report on Progress

Charge density waves in strongly correlated electron systems

Chih-Wei Chen[1], **Jesse Choe**[2] **and E Morosan**[1,2]

[1] Department of Physics and Astronomy, 6100 Main Street, Rice University, Houston, TX 77005, USA
[2] Department of Electrical and Computer Engineering, 6100 Main Street, Rice University, Houston, TX 77005, USA

E-mail: emorosan@rice.edu

Received 1 November 2015, revised 14 March 2016
Accepted for publication 21 March 2016
Published 4 July 2016

Abstract

Strong electron correlations are at the heart of many physical phenomena of current interest to the condensed matter community. Here we present a survey of the mechanisms underlying such correlations in charge density wave (CDW) systems, including the current theoretical understanding and experimental evidence for CDW transitions. The focus is on emergent phenomena that result as CDWs interact with other charge or spin states, such as magnetism and superconductivity. In addition to reviewing the CDW mechanisms in 1D, 2D, and 3D systems, we pay particular attention to the prevalence of this state in two particular classes of compounds, the high temperature superconductors (cuprates) and the layered transition metal dichalcogenides. The possibilities for quantum criticality resulting from the competition between magnetic fluctuations and electronic instabilities (CDW, unconventional superconductivity) are also discussed.

Keywords: strongly correlated electron systems, charge-density waves, cuprates, superconductivity, transition metal dichalcogenides

(Some figures may appear in colour only in the online journal)

1. Glossary of acronyms

AFM: Antiferromagnetic
ARPES: Angle resolved photoemission spectroscopy
BCS: Bardeen–Cooper–Schrieffer
CCDW: Commensurate charge density wave
CDW: Charge density wave
FM: Ferromagnetic
FWHM: Full width at half maximum
ICDW: Incommensurate charge density wave
QCP: Quantum critical point
r.l.u: reciprocal lattice units
RXS: Resonant x-ray scattering
RIXS: Resonant inelastic x-ray scattering
SC: Superconductivity
SCES: Strongly correlated electron system
SDW: Spin density wave
SPM: Scanning probe microscopy
STM: Scanning tunneling microscopy
TEM: Transmission electron microscopy
TMD: Transition metal dichalcogenide

2. Introduction

One of the cornerstones of solid state physics is the free electron theory, which models the electrons in a condensed matter system as entirely non-interacting. By adding corrections to this model in the form of the periodic lattice potential, the theory becomes the nearly free electron theory and is more accurate in describing real material systems, including metals, semiconductors, and insulators. However, there are classes of

materials that cannot be explained by the free or nearly free electron theory which do not take electron-electron interactions into account. In heavy fermion systems, hybridization occurs between the *f*-shell and the conduction electrons, often leading to large electron mass renormalization [1]. Electron-phonon interactions can result in an attractive potential between two electrons, and thus the formation of coherent Cooper pairs in BCS superconductors [2] as a way of resolving a Fermi surface instability. Charge density waves (CDWs) are also the result of instabilities at the Fermi energy, in this case resolved by energy minimization through a periodic lattice modulation [3]. In a similar manner, spin density waves (SDWs) consist of modulations of the magnetic moment instead of electron density [4]. Not surprisingly, many of these strongly correlated electronic states coexist or compete in the same materials: the iron pnictides often show SDW and unconventional superconductivity (SC) mediated by magnetism; in heavy fermions, the magnetic order is often suppressed by a superconducting ground state; and transition metal dichalcogenides (TMDs) and cuprates can show both SC and CDW behavior. A common thread across these classes of strongly correlated materials is the superconducting dome (or optimal SC) often protecting a quantum critical point (QCP) where the ground state (magnetic order or density wave) is suppressed to $T = 0$ K.

A CDW can be easily envisioned in a low dimensional system. It is known that any new periodicity in the crystalline lattice of a metal results in a gap opening in the Fermi surface. However, the lattice distortions are typically prevented by Coulomb repulsion, unless the Coulomb energy penalty is more than compensated for by the lowering of the overall energy through the opening of a large enough gap. This is exactly the scenario which, in one dimensional systems, favors a lattice modulation below a critical temperature. Peierls showed [5] that a metal-to-insulator transition takes place at this critical temperature in a one dimensional material because of the electron–phonon coupling, and that this transition is expected to be second order. This scenario is rooted in the Fermi surface nesting (figure 1(a)) which results in a diverging generalized Lindhard susceptibility $\chi(\mathbf{q})$ (figure 1(b)) for $\mathbf{q}$ corresponding to the nesting vector. The first experimental evidence for CDW transitions was indeed unveiled in 1D systems, including the transition metal chalcogenides MX_3 (M = Nb and Ta, X = S, Se, or Te) [6, 7], halogen transition metal tetrachalcogens $(MX_y)_nh$, such as $TaSe_4I$ [8], the blue bronzes $A_{0.3}MoO_3$ (A = K and Rb) [9], and Krogmann's salt $K_2Pt(CN)_4Br_{0.3}{\cdot}3.2H_2O$ [10, 11]. Although the Lindhard function divergence takes place strictly for systems with one dimensional Fermi surfaces (red curve in figure 1(b)), the sharp inflection for the 2D case (blue curve) already hints at the possibility of Fermi surface nesting-driven CDW transitions in materials with highly anisotropic band structures (both 1D and 2D). This is indeed a common occurrence in the layered TMDs, the cuprates, and the rare earth tellurides R_2Te_5 (R = rare earth) [12–14]. CDW behavior has also been observed in three dimensional systems, particularly in the rare earth and alkaline earth intermetallics such as $R_5Ir_4Si_{10}$ [15–17], $R_2Ir_3Si_5$ [18], RPt_2Si_2 [19], RTe_3 [20] (R = rare earth), and the $M_3T_4Sn_{13}$ (A = Ca, Sr; T = Ir, Rh) system

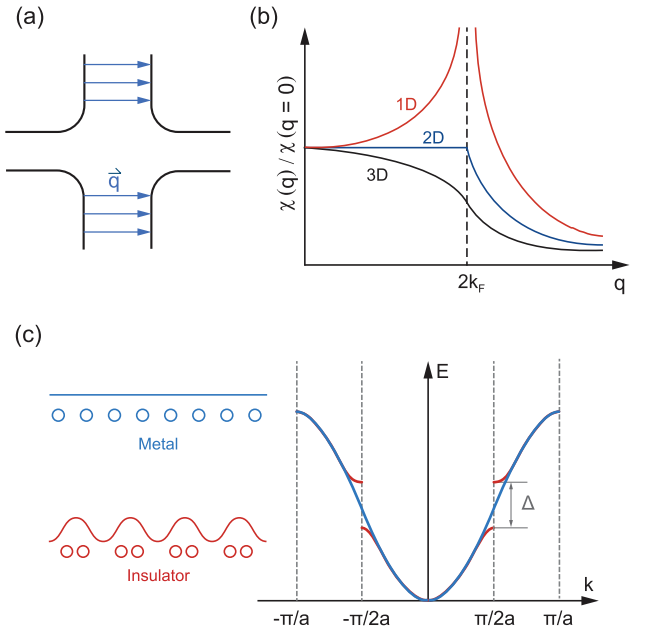

Figure 1. (a) An illustration of Fermi surface nesting with a wavevector $\mathbf{q}$. (b) The $T = 0$ Lindhard response function $\chi(\mathbf{q})$ as a function of wavevector $\mathbf{q}$ for one-, two-, and three-dimensional free electron gases. (c) Schematic representation of a Peierls transition in a one-dimensional material, with the structure and dispersion before (after) the Peierls transition represented in blue (red). A gap Δ opens up at the wavevector $q = 2k_F$ corresponding to the new lattice periodicity.

[21, 22]. While the CDW mechanism in these materials is not well understood, the CDW transition tends to be first instead of second order. In addition, the CDW appears as quasi-1D despite the 3D crystal structure.

This paper focuses on the correlations associated with the CDW, a periodic modulation of the conduction electron density that particularly arises in low dimensional (one or two dimensional) bulk systems [3]. While CDW systems are studied for their intrinsic properties such as nonlinear electrical conduction [7] as well as the relationship between the electrical states and the crystal structure, we will focus on their significance in relation to other strongly correlated states, both magnetic and electronic. After a brief overview of the origin of the CDW transition, we will survey the experimental and theoretical manifestations of such transitions, and finally the interplay and competition between CDWs and other correlated states in two classes of materials: the cuprates and TMDs. More specifically, we will look closely at the competition between the CDW and SC in hole- and electron-doped cuprate superconductors. In TMDs, we will cover the CDW and SC interplay as a function of control parameters such as pressure, doping and intercalation with non-magnetic elements, as well as the correlation effects resulting from intercalation of magnetic elements.

3. Mechanisms underlining the CDW transition

This section is dedicated to a review of conventional and unconventional mechanisms behind the CDW transition. Specifically, we will review Fermi surface nesting and its

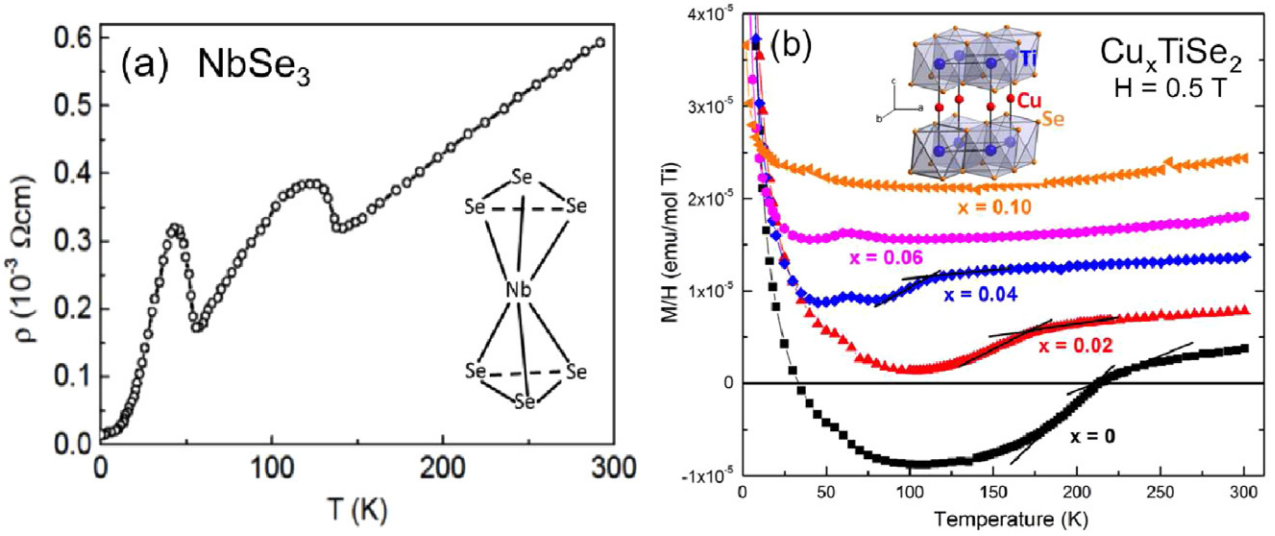

Figure 2. (a) Electrical resistivity of $NbSe_3$ showing two CDW transitions around 130 K and 40 K [6]. Reprinted with permission from [6], copyright 1976 Elsevier. (b) Magnetic susceptibility of Cu_xTiSe_2 showing the CDW transition (marked by the solid lines) decreasing with the amount of intercalated Cu [39]. Reprinted with permission from [39], copyright 2006 Nature Publishing Group.

role in the Peierls transition in 1D systems, followed by a comparison between this and other electron–phonon coupling instabilities, such as BCS superconductivity. With ample evidence for the existence of CDW transitions beyond one dimension, it is necessary to survey possible mechanisms beyond electron–phonon coupling in 2D and 3D systems. This review will touch upon two such theories: the excitonic insulator and the Jahn–Teller effect.

3.1. CDW transitions driven by Fermi surface nesting

In 1D systems, a CDW is a modulation of the electron density ρ with a wave vector $\mathbf{q}$:

$$\rho(\mathbf{r}) = \rho_0 + \rho_1 \cos(\mathbf{q}\cdot\mathbf{r} + \phi), \tag{1}$$

where ρ_0 is the unperturbed electron density, which in simple metals is a constant (figure 1(c)), ρ_1 is the amplitude of the modulation, and ϕ is the phase of the CDW.

For a time-independent potential, the charge density can be written as [23]:

$$\rho^{\text{ind}}(\mathbf{q}) = \chi(\mathbf{q})\phi(\mathbf{q}), \tag{2}$$

where $\mathbf{q}$ is the wavevector, and $\chi(\mathbf{q})$ is the Lindhard response function:

$$\chi(\mathbf{q}) = \int \frac{\mathrm{d}\mathbf{k}}{(2\pi)^d} \frac{f_{\mathbf{k}} - f_{\mathbf{k}+\mathbf{q}}}{\epsilon_{\mathbf{k}} - \epsilon_{\mathbf{k}+\mathbf{q}}}, \tag{3}$$

with $f_{\mathbf{k}} = f(\epsilon_{\mathbf{k}})$ the Fermi–Dirac function.

In some (often one- or two-dimensional) systems, Fermi surface nesting can lower the system's energy. Fermi surface nesting occurs when large, parallel regions of the Fermi surface are connected by a single wavevector $\mathbf{q}$ (figure 1(a)), in which case the $\epsilon_{\mathbf{k}}$ and $\epsilon_{\mathbf{k}+\mathbf{q}}$ energies are degenerate. In one-dimensional systems, when $q = 2k_F$ the energy is lowered via a lattice distortion known as a Peierls transition: when sufficiently large parts of the Fermi surface are nested by a wavevector $2k_F$ ($\epsilon_{\mathbf{k}} = \epsilon_{\mathbf{k}+2\mathbf{k}_F}$), the denominator in equation (3) vanishes and the Lindhard response function diverges. This indicates that the electronic structure is not stable, and any small perturbation will cause a charge density redistribution or Fermi surface reconstruction. Most importantly, periodic lattice modulation can overcome the Coulomb repulsion by lowering the system's energy as a gap opens at the Fermi level. The lattice distortion drives the conduction electron's density periodic modulation, known as a charge density wave. Because of the Fermi surface gap opening, the Peierls transition is accompanied by a metal-to-insulator transition. When the periodicity of the electron density is a rational multiple of that of the lattice distortion, it gives rise to a commensurate CDW (CCDW). When the ratio of the two periodicities is a irrational number, the result is an incommensurate CDW (ICDW), resulting in an electron density which is out of phase to the lattice distortion.

CDWs were originally thought to only exist in one-dimensional systems and arise solely due to lattice distortions (Peierls transitions). However, He and Zhang [24] showed that the CDW in $NbSe_3$ (figure 2) has a pseudogap above the highest known Peierls transition temperature. This suggested that CDWs might not be solely driven by lattice distortions, and electron-electron interactions could also play an important role in the formation of CDWs. Furthermore, the discovery of CDW in 2D [25] and 3D [22, 26] systems made it apparent that mechanisms other than phonon-electron interactions can lead to the formation of CDWs.

While CDWs are of interest from a fundamental point of view, their close relationship with other correlated electronic phenomena, such as superconductivity, sparks further interest [27]. Comparing the Peierls transition to conventional superconducting transitions, it is worth noticing that they are both driven by electron–phonon interactions which cause instabilities at the Fermi surface and the formation of a gap. In a Peierls transition, the CDW state occurs as a coupled electron–phonon condensate. In contrast, electrons in conventional superconductors form Cooper pairs, and the superconducting state is an electron pair condensate. Qualitatively,

the formalism describing the transition temperatures of both phenomena are very similar. The Peierls transition temperature T_P, derived from mean-field theory [23], is of the form:

$$k_B T_P = 1.14\epsilon_F \exp[-\frac{1}{Vg(\epsilon_F)}]. \quad (4)$$

and the BCS superconducting transition temperature [2] is:

$$k_B T_c = 1.14\epsilon_D \exp[-\frac{1}{Vg(\epsilon_F)}], \quad (5)$$

where V is the electron–phonon coupling constant, and ϵ_F and ϵ_D are the Fermi and Debye energies, respectively. It is readily apparent that T_P temperatures can be two to three orders of magnitude larger than T_c values, given that they scale with the Fermi ($\epsilon_F \sim 1$ to 10 eV) and Debye ($\epsilon_D \sim 0.01$–0.1 eV) energies respectively. However, electron–phonon interactions alone are not enough to account for either the CDW or the superconducting ground state. This is indicated by the discovery of the high CDW onset temperature in $NbSe_3$ [6], CDW states in 2D systems and their competition with SC [28, 29], as well as the unconventional SC observed in heavy fermion systems [30], the cuprates [31], and the iron pnictides [32]. Moreover, it has been shown that the CDW and superconducting states are significantly correlated in cuprates [13], suggesting that the understanding of the CDW mechanism in these and other strongly correlated systems would be key to revealing the underlying mechanisms for high temperature superconductivity.

3.2. Unconventional mechanisms for CDW formation

1D CDWs are effectively described by the Peierls transition and Fermi surface nesting. However, in 2D systems, there are situations where this description fails, particularly since the Lindhard function only diverges at $\mathbf{q} = 2\mathbf{k}_F$ in 1D systems, while in 2D systems there is a sharp slope change at the nesting wavevector (figure 1(b)). As a result, various alternative explanations for the CDW formation in non-1D systems have been put forth. While for numerous materials, electron–phonon coupling appears to be the underlying cause of CDW formation, [33, 34] there are notable exceptions. $TiSe_2$ is one prominent such exception: this 2D TMD does not show Fermi surface nesting [35], calling for different scenarios to explain the CDW formation in this and other (2D or 3D) compounds. Below we discuss the excitonic insulator [36] and the Jahn–Teller effect [37] as two possible hypotheses that have been probed in the context of $TiSe_2$.

The excitonic insulator mechanism was proposed by Jerome *et al* [36]. In a semiconductor with a small band gap or a semi-metal with a small band overlap, there exist only a small number of charge carriers. These carriers can form excitons, bound states of holes and electrons, as long as the indirect positive (semiconductor) or negative (semi-metal) gap is smaller than the exciton binding energy. This removes charge carriers from the Fermi surface and creates an insulating state. For an indirect gap, this results in a non-zero exciton momentum, and in turn a CDW transition [37].

The band Jahn–Teller effect, first proposed by Hughes, is driven by a structural distortion which breaks the degeneracy of the ground state energy [38]. As an example, the transition metal T in the TX_2 dichalcogenides can be in either octahedral (1T) or trigonal prismatic (2H) T-X_6 coordination (the different polytypes in TX_2 systems are discussed in detail in section 5.2). The transition metal d bands have different energies for the octahedral or trigonal prismatic T-X_6 coordination, with the 2H polytype having a lower d_{z^2} energy than the 1T polytype. Therefore, the energy of the octahedral polytype could be lowered by a transition to a trigonal coordination, when the chalcogen ions X above and below a transition metal ion, T, in the octahedra rotate in opposite directions. This results in a local increase in the conduction electron density (negative charge) at the unit cell corners, which becomes an attractive potential for the positively charged T ions. The result is a lattice distortion driven by a real-space T-X coordination making it a band Jahn–Teller effect rather than a Fermi surface effect.

4. Experimental and theoretical signatures of CDW transitions

Upon cooling, the CDW transition opens up a gap at the Fermi surface, resulting in the decrease of the number of charge carriers. In turn, this yields an increase of the electrical resistivity upon cooling below the CDW transition, as exemplified in figure 2(a) for $NbSe_3$ [6]. Concurrently, the magnetic susceptibility associated with the conduction electrons decreases at the CDW transition, as illustrated by the Cu-intercalated $TiSe_2$ (figure 2(b)) [39]. Signatures of CDW behavior can also be extracted from Raman spectroscopy as a strong dependence on photon polarization and on characteristic wave vectors, [40] and optical conductivity [41].

These phase transitions, however, do not uniquely identify the ground state as a CDW and additional microscopic probes are often useful to visualize the CDW state, while scattering techniques can directly determine the structural transition and the Fermi surface details. Scanning probe microscopy measurements can be performed to give a picture of the local density of states and the Fermi surface [42], while angle resolved photoemission spectroscopy (ARPES) [43] can directly image the Fermi surface [44]. The experimental results can then be contrasted with band structure calculations, which can identify possible nesting vectors.

Figure 3 illustrates a comparison between (a) ARPES, (b)–(c) the real part of the Lindhard function, and (d) Fermi surface plots for three chalcogenides with similar nesting vectors: 2H-$TaSe_2$ (top), 2H-$NbSe_2$ (middle) and Cu-intercalated 2H-NbS_2 (bottom). The three compounds chosen for this comparison have very different CDW behavior. 2H-$TaSe_2$ displays both ICDW and CCDW transitions upon cooling below 125 K, and 90 K respectively [45], while only a ICDW state sets in for 2H-$NbSe_2$ at a much lower temperature ($T_{CDW} < 33$ K) [29], and no CDW transition is apparent in either pure or Cu-intercalated 2H-NbS_2. The Lindhard response function reveals a surprising lack of correlation between the generalized susceptibility and the CDW temperature, as the highest $\chi_{0,max}$ (figure 3(b))

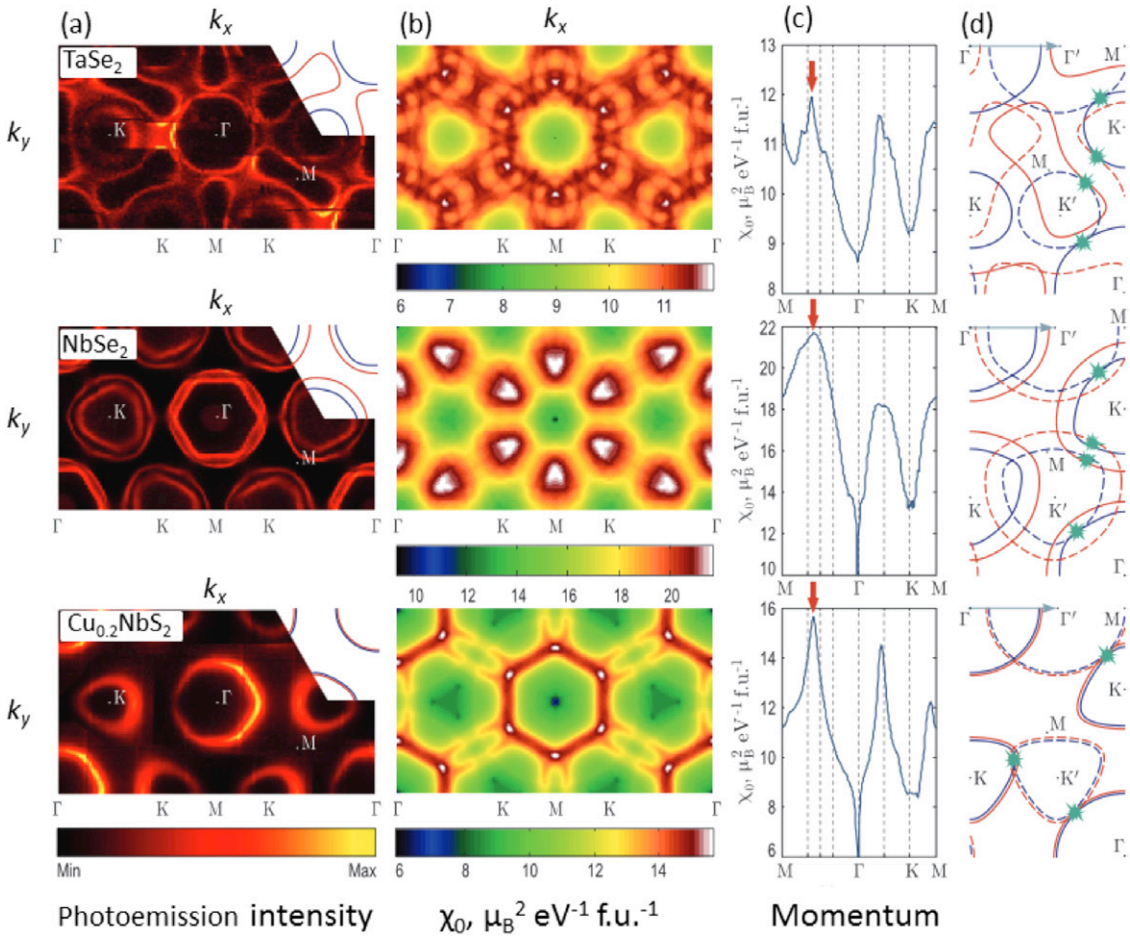

Figure 3. Fermi suface nesting in 2H-$TaSe_2$ (top), 2H-$NbSe_2$ (middle), and 2H-$Cu_{0.2}NbS_2$ (bottom). (a) ARPES measurements of the Fermi surface. (b) Real part of the Lindhard function as a function of momentum, with the dominant nesting vector represented by white spots and (c) marked by red arrows in the profiles along high symmetry directions. (d) Fermi surface nesting vectors (arrows at the top of each panel) and the corresponding nested Fermi surface sheets shown in solid and dashed lines (reproduced with permission from [44], copyright 2008 IOP Publishing).

occurs for the system with intermediate T_{CDW} (2H-$NbSe_2$), and the compound with the highest T_{CDW} (2H-$TaSe_2$) has the lowest $\chi_{0,max}$. This disparity becomes even more remarkable upon the observation that the dominant nesting vector is identical in all three compounds, indicated by the red arrows in figure 3(c). The Fermi surface plots in figure 3(d) reveal the different nesting configurations, and point towards differences between electron–phonon coupling or out of plane dispersion as possible ways of reconciling the differences and similarities in the CDW properties of the three selected compounds.

While transport and magnetization transitions (figure 2), together with band structure and Fermi surface data indicate a CDW transition, the lynch pin to the CDW ground state argument is the presence of a superstructure resulting from the modulation of the ionic lattice. Evidence for such superstructures can be provided by diffraction and real space imaging techniques such as scanning tunneling microscopy (STM) [46, 47] or atomic force microscopy (AFM) [48]. X-ray scattering, the most accessible scattering technique, proves problematic in the detection of CDW transitions because of the x-ray energy-dependent penetration length. When using long wavelength x-rays, the penetration length is short and may not be able to collect enough signal, which causes weak diffraction spots. For shorter wavelength x-rays, the penetration length is longer but the wavelength may be too short compared to the CDW periodicity. In both cases, CDWs that have long periodicity or small wavevectors are hard to detect with x-ray diffraction.

Resonant x-ray scattering (RXS) represents a viable alternative, since it uses x-rays with the energy tuned to the absorption edge of a specific element, where the scattering cross section is significantly enhanced [49]. By using RXS, one can detect charge, spin, or orbital ordering of a specific element [49, 50]. Furthermore, because RXS is sensitive to the valence electrons, it is widely used to study the charge modulation of specific elements in a variety of systems [51–53]. An extension of RXS, resonant inelastic x-ray scattering (RIXS) can be used to study elementary excitations such as CDWs, orbital excitations, or magnetic excitations [54]. RIXS is a complementary technique to inelastic neutron scattering experiments and exploits both energy and momentum space. Due to the photon energy region that is used in RIXS, it can measure the full dispersion of low-energy excitations which is difficult by using inelastic neutron scattering [54]. For CDWs in cuprates, RIXS shows that when the momentum transfer is tuned to the period of CDWs, the spectrum weight of specific energy transfer is increased [55].

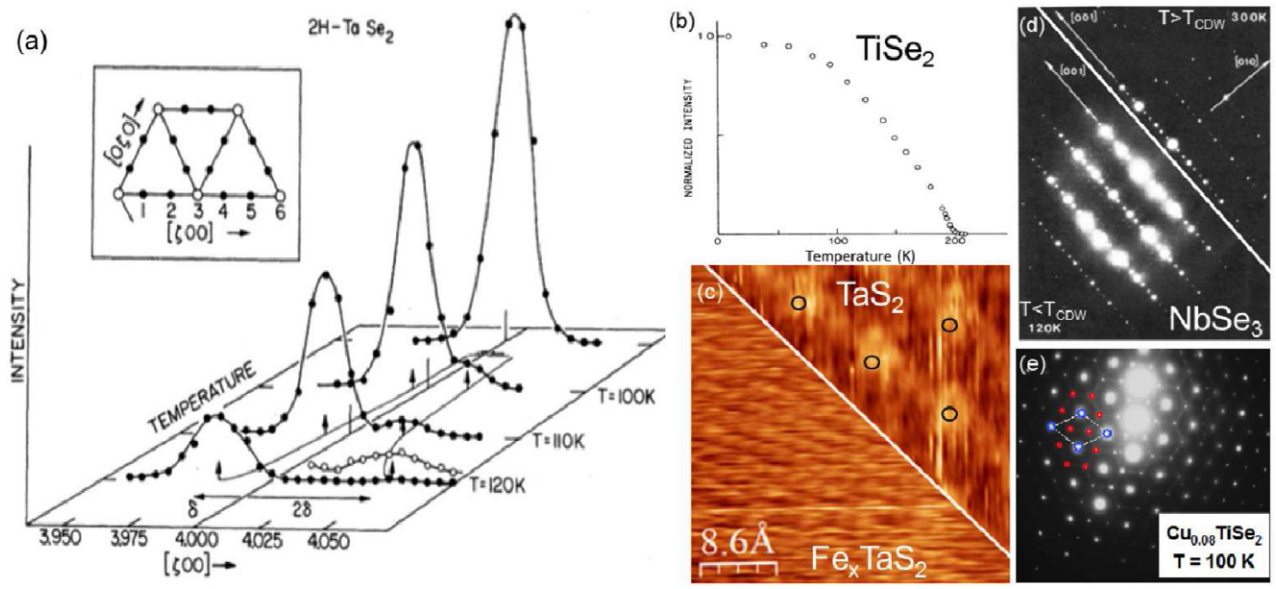

Figure 4. (a)–(b) Neutron diffraction data for 2H-$TaSe_2$ (reproduced with permission from [57], copyright 1975 APS) and $TiSe_2$ (reprinted with permission from [25], copyright 1976 APS). (c) The CDW superstructure in TaS_2 (top) is destroyed by the Fe intercalation (bottom) ([58]). Electron diffraction images for (d) $NbSe_3$ above (top) and below (bottom) T_{CDW} (reprinted with permission from [116], copyright 1978 IOP Publishing) and (e) $TiSe_2$, with the main and superstructure reflections marked in blue and red respectively.

Because neutrons are charge neutral, they do not interact with the electronic charges directly. Instead, neutron scattering detects CDWs through measuring the crystallographic modulation [12, 56]. Neutrons have a longer penetration length than x-rays for wavelengths close to the periodicity of the CDW, elastic neutron scattering is suitable for measuring small wave vector CDWs. Additionally, inelastic neutron scattering is also suitable to measure the energy spectrum of the CDW and the gap formed by the CDW [56]. Overall, neutron scattering has a detectable energy transfer when its wavevector matches the wavevector of the CDW.

Very early neutron diffraction experiments on the layered TMDs [57] provided the first insights into the Kohn anomaly signatures for the CDW compounds 2H-$TaSe_2$ (figure 4(a)) and 2H-$NbSe_2$ (not shown). Moncton and Axe [57] showed that, upon cooling, 2H-$TaSe_2$ goes into a ICDW state, with a very small departure from commensurability (denoted as $\delta \sim 2\%$). Upon further cooling, a weak first order transition takes the system into a CCDW state, while in the ICDW state an additional weaker distortion (open symbols in the main panel of figure 4(a)) is registered. By contrast, as mentioned before, 2H-$NbSe_2$ displays only an ICDW state, remarkably with an identical δ value. Even more surprising is that 1T-$TiSe_2$ [25] shows only a transition to a CCDW around $T = 220$ K, with the normalized intensity as a function of temperature shown in figure 4(b).

Electron diffraction images for the quasi-1D chalcogenide $NbSe_3$ and layered Cu-intercalated $TiSe_2$ in figures 4(d) and (e) show the [0 0 1] superstructure in the former compound upon cooling through the CDW transition, while in the latter a $2a$, $2c$ superstructure is revealed at low T by the additional weak spots (red) around the strong Bragg reflections (blue).

Real space images of the superstructure formation can be equally informative with regards to the CDW transition and wavevector. Figure 4(c) (top) shows the CDW in TaS_2 as a modulation on a scale far too large to be that of the atomic corrugation. Figure 4(c) (bottom) indicates that the CDW and its corresponding lattice modulation are destroyed by the intercalation of Fe and the underlying atomic periodicity is revealed.

5. CDWs in strongly correlated electron systems

5.1. CDWs and other correlated electron states in the cuprates

Similar to the Peierls transition, conventional SC is driven by lattice distortions. However, in superconductors, the associated attractive potential results in Cooper pair formation (an instability in the particle-particle channel), while in CDW systems this distortion is associated with an instability in the particle-hole channel. One important consequence is that the two states (CDW and SC) are often in competition in the same compounds [59, 60], and can even coexist in some instances [39]. However, strong electron correlations could also to lead to unconventional SC or CDW transitions. For the latter, we already mentioned the excitonic insulator or band Jahn–Teller effect (section 3.2) as possible CDW mechanisms other than the Peierls structural distortion. The discovery of superconductivity in heavy fermions [30], cuprates [31], and more recently, iron pnictides [32], prompted the need for mechanisms beyond the BCS theory to describe unconventional superconductivity. In these systems, it is believed that magnetic correlations [61] and not phonons mediate the Cooper pairing. This takes place when the magnetic order is suppressed by some extrinsic parameter such as magnetic field, doping, or pressure, towards a dome of superconductivity which, in turn, often 'protects' a QCP where the magnetic order goes to zero. This is exemplified in the phase diagram for doped cuprates in figure 5(c), with electron (hole) doping increasing to the left (right). Recent experiments have shown that,

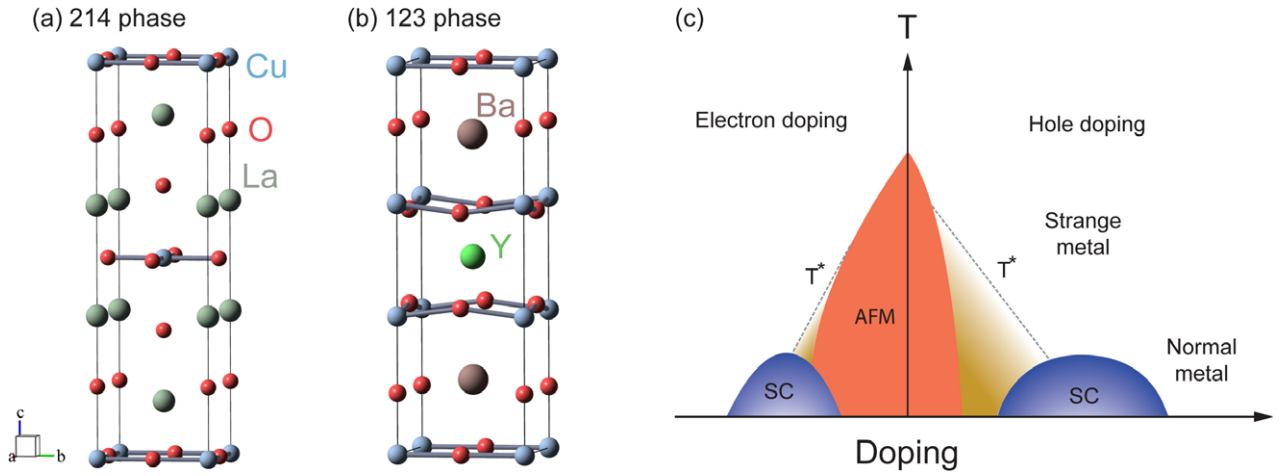

Figure 5. (a) Crystal structure of La_2CuO_4 (214 phase). (b) Crystal structure of $YBa_2Cu_3O_7$ (123 phase). (c) Schematic temperature versus doping phase diagram for cuprates.

in unconventional superconductors, different electron correlations and ordered states compete with superconductivity [12, 13, 62, 63]. Because these symmetry-breaking orders appear at similar temperatures, it was proposed that they were entangled and could be considered as *intertwined orders* [63]. Additionally, the re-entrance of the long-range order upon the suppression of superconductivity indicates that these orders are competing for the same electrons close to the Fermi surface. Therefore, understanding this competition will reveal more about electron correlations and help draw a clearer picture of the pairing mechanism in unconventional superconductors.

Early measurements show that spin and charge densities are modulated in the hole-doped cuprates, e.g. doped La_2CuO_4 (referred to as '214', figure 5(a)). These modulations give rise to *stripe order* [12]. In cuprates, specific hole-doping concentrations, together with a low-temperature orthorhombic-to-tetragonal structural phase transition, result in the suppression of superconductivity. A long-standing question, known as the '1/8 problem', has to do with the anomalous suppression of superconductivity in the hole-doped '214' cuprates, which has been attributed to strong charge and spin order effects in $La_{1.6-x}Nb_{0.4}Sr_xCuO_4$, when the hole doping concentration p in the CuO_2 plane is equal to 1/8. [12].

Recently, a CDW was observed in $YBa_2Cu_3O_{6+\delta}$ (YBCO, referred to as the '123' phase, figure 5(b)) when the magnetic field suppressed the SC [13]. As was the case in '214', the charge density order in '123' has the highest transition temperature close to 1/8 hole doping, where the superconductivity transition temperature is partially suppressed. This suppression results in two SC domes, and suggests a possible QCP at this concentration ($p = 1/8$). After the discovery of CDWs inside the SC dome, the CDW was also observed outside of the superconductivity dome *and* in the pseudogap region of (Y, Nd)$Ba_2Cu_3O_{6+\delta}$ by using hard x-rays [51, 64] and soft x-ray scattering [52, 65, 66]. These results are testament to the comparable energy scales of the CDW and SC.

The similarities and differences between hole-doped '214' and '123' phases provide clues toward understanding the electron correlations in cuprates. Both phases have the strongest charge modulations at the 1/8 doping, where T_c is reduced from the optimal value. In the '214' phase, the SC is almost completely suppressed and the charge modulations have maximum order parameter at $p = 1/8$, as observed in $La_{1.875}Ba_{0.125}CuO_4$ [62]. In the '123' phase, the SC is slightly suppressed and there is a plateau of T_c around $p = 1/8$ as observed in $YBa_2Cu_3O_{6.6}$ [62]. Meanwhile, the differences in the CDWs in both phases can also be seen by comparing the same '214' and '123' compositions with the strongest CDWs, $La_{1.875}Ba_{0.125}CuO_4$ and $YBa_2Cu_3O_{6.6}$. In the $La_{1.875}Ba_{0.125}CuO_4$ compound, the wave vector of the CDW is ~0.24 reciprocal lattice units (r.l.u.) along both H and K directions [53, 62]. By contrast, the wavevector of $YBa_2Cu_3O_{6.6}$ is ~0.31 r.l.u., and there is a small anisotropy between the H and K directions [53]. Furthermore, the charge modulation in $La_{1.875}Ba_{0.125}CuO_4$ has a larger order parameter value than the one in the $YBa_2Cu_3O_{6.6}$, which indicates that the CDW is more developed in the former compound. It can also be seen that the CDW in $YBa_2Cu_3O_{6.6}$ under zero field is incomplete and the SC is only partially suppressed by the CDW. The CDW also has a different correlation length in these two phases,~250 Å in the doped '214', and ~50 Å in the doped '123' [53]. Both the magnitude of the order parameter and the correlation length indicate that the CDW in $La_{1.875}Ba_{0.125}CuO_4$ is stronger and extends wider than the one in $YBa_2Cu_3O_{6.6}$. These facts are further connected to the suppression of SC, and provide a partial explanation for the faster suppression of T_c in $La_{1.875}Ba_{0.125}CuO_4$ compared to $YBa_2Cu_3O_{6.6}$ [62], while emphasizing the competition between the CDW and SC states in both doped cuprates.

In light of the asymmetrical behavior with hole- or electron-doping in cuprates (figure 5), the difference between the CDWs in the two types of cuprates is important for understanding the competition with SC. Recently, RXS in electron-doped $Nd_{2-x}CeCuO_4$ [67] revealed the presence of a CDW. The results show that the CDW has a wavevector ~0.24 r.l.u. along the H direction, which is close to the wavevector observed in hole-doped $La_{1.875}Ba_{0.125}CuO_4$. Additionally, the ordering temperature T_{CDW} in electron-doped $Nd_{2-x}CeCuO_4$ is ~340 K, higher than the pseudogap onset temperature. The

hole-doped $La_{1.875}Ba_{0.125}CuO_4$ has its T_{CDW} close to or lower than the onset temperature of the pseudogap. Furthermore, the full width at half maximum (FWHM) of the RXS charge order peaks suggests a correlation length between 15 Å and 27 Å, an order of magnitude smaller than in hole-doped $La_{1.875}Ba_{0.125}CuO_4$. Therefore it appears that the electron-doped '214' $Nd_{2-x}CeCuO_4$ phase has a higher T_{CDW} and smaller correlation length than the corresponding values in the hole-doped '214' $La_{1.875}Ba_{0.125}CuO_4$.

CDW instability and CDW fluctuations are suggested to be correlated with d-wave superconductivity [68]. These CDW instabilities and fluctuations may result in the large scattering of quasiparticles near the Fermi surface in cuprates [69]. Owing to the fact that CDWs and SC are entangled in cuprates, understanding the origin of the CDW transition in these systems may offer clues into their unconventional high temperature SC. It has been suggested that the CDW in cuprates results from the antinodal Fermi surface [46]. However, a recent study of the CDW in $Bi_2Sr_{2-x}La_xCuO_{6+\delta}$ indicates a more complicated CDW mechanism [26]. Without including the self-energy, which combines the features found from the diagonalization of the Hubbard model with doping-dependent parameters, their band structure calculations result in an antinodal Fermi surface nesting wave vector close to (0, 0.139, 0). This value is different from the observed CDW vector $\mathbf{q}_{CDW} \sim (0, 0.265, 0)$ determined from RXS. However, after considering the self-energy, the calculations result in an Fermi surface arc, which was confirmed by ARPES measurements. The nesting vector between the Fermi arcs is ∼(0, 0.265, 0), which is close to the observed wavevector of the CDWs. Because the self-energy is correlated with the pseudogap, these experimental and theoretical results suggest that the CDW and pseudogap are correlated, at least in $Bi_2Sr_{2-x}La_xCuO_{6+\delta}$, and likely in most cuprates. In $Bi_2Sr_{2-x}La_xCuO_{6+\delta}$, the CDW onset temperature is close to the onset temperature of the pseudogap, which further supports the scenario of correlated pseudogap-CDW formation mechanisms. However, to generalize this argument to other cuprates more experimental data is needed because in many cases, the onset temperatures of the CDW and pesudogap are distinct. For example we see in figure 6 that the onset temperatures for YBCO, T_{CDW} (red circles) and the pseudogap temperature T^*(grey triangles), are vastly different. The driving mechanism for CDWs in cuprates, and the correlations between CDWs and superconductivity are still the subject of active research, even as we approach the three decade anniversary of the discovery of high temperature SC.

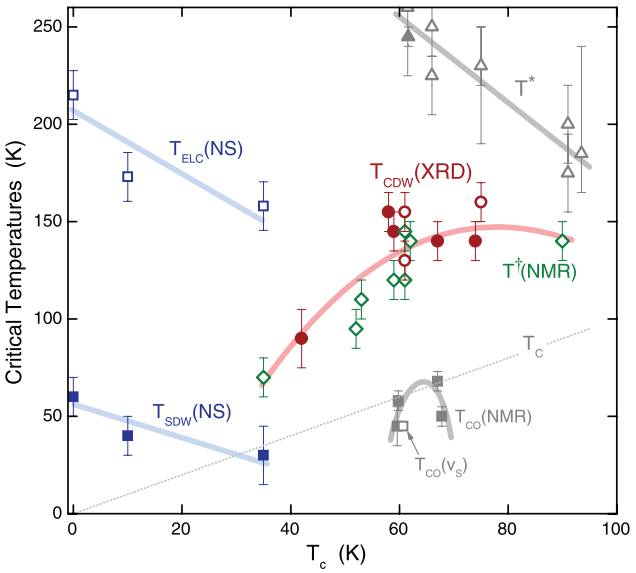

Figure 6. Long range spin or charge order versus superconductivity temperatures in YBCO showing the onset temperature for charge density wave (T_{CDW}), charge order (T_{CO}), Spin density wave (T_{SDW}), electronic liquid crystal state (T_{ELC}), and pseudogap (T^*) (reproduced with permission from [62], copyright 2014 APS).

5.2. Competition between CDWs and other correlated electron states in TMDs

The great variety of phenomena in correlated electron systems is exemplified by the layered TMDs, TX_2 (T = transition metal, X = S, Se, or Te). These materials form X-T-X layers bound together by van der Waals forces, resulting in a quasi-2D system. Transition metal dichalcogenides have already found a variety of uses from chemical catalysis [70], lubricants [71], electrodes for batteries [72], and in nanotechnology [73, 74]. These systems have some structural similarities to graphite, which is formed of hexagonal layers of graphene stacked and bound in a similar manner by van der Waals forces. Graphene has been a hot topic of research for its high electrical and thermal conductivity and optical transparency [75, 76].

While no TMDs have been found to match graphene's desirable properties (mainly large mechanical strength, electrical conductivity), they hold several advantages over graphene that make them an attractive area of research. Industrial applications for graphene are typically limited by the problem of growing graphene at a high enough quality in large quantities [75]. In contrast, TMDs are relatively easy to grow and TMDs such as MoS_2 are already used in industrial applications [71]. TMDs also have the advantage of being made of two atoms, a transition metal and a chalcogen, and the combinations of possible T (T = Ti, V, Zr, Nb, Mo, Hf, Ta, W), X (X = S, Se, Te), and their different polytypes [77] yields over 40 known TMDs. Graphene is also a zero gap semiconductor, which requires inducing a gap to make it into a viable transistor. With TMDs, by simply changing either the transition metal, the chalcogen, or both, one can alter their properties. TMDs run the gamut from insulators (HfS_2) [78], semiconductors (MoS_2) [74], semi-metals (WTe_2, TcS_2) [79], to metals (NbS_2, VSe_2) [80]. Having a X-T-X layer instead of a single layer of carbon (as is the case with graphene) allows the formation of either octahedral or trigonal prismatic T-X polyhedra (figure 7(a)). The layers can then stack in different configurations, resulting in multiple polytypes, with some examples schematically shown in figures 7(b) and (c). Multiple polytypes of the same material exist which can drastically alter the TX_2 properties. For example, in the TaS_2 system, the 1T-TaS_2 polytype does not show SC but the 2H-TaS_2 polytype does [60]. Finally, the TX_2 systems maintain many of the appealing properties of graphene, like the layered structure ideal for making thin film devices [73] and the ability

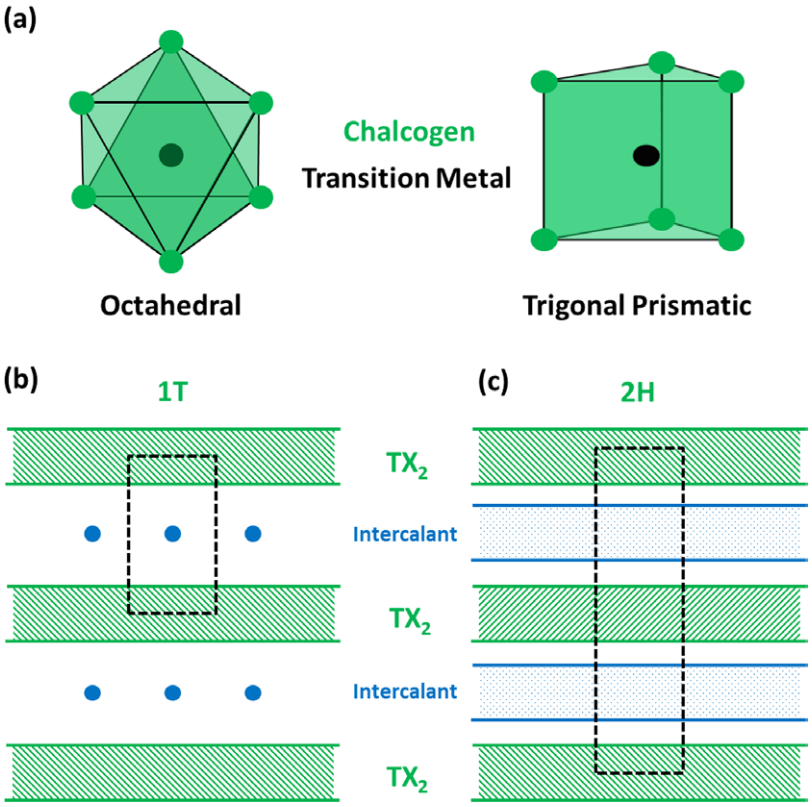

Figure 7. TX_2 polytypes (unit cell outlined in black) result from (a) different coordination T-X_6 polyhedra (octahedral or trigonal prismatic) and the stacking of the TX_2 layers. (b) One layer in a trigonal unit cell forms the 1T polytype, while (c) in the 2H polytype, the layers are staggered along the *c* axis, resulting in a hexagonal unit cell with 2 layers per unit cell. Other TX_2 polytypes include 3R (rhombohedral), 4H, and 6R.

to easily intercalate atoms between layers [81]. Even though no TMDs have been found to match the electrical properties of graphene, the diversity and tunable parameter space in the TMDs makes them a far better playground for studying 2D systems, and more practical for electronic applications.

MoS_2 is a prime example of the versatility the TMDs hold for applications. It is commonly used as an industrial lubricant [71, 82], but recent interest has been focused on its electrical properties, as an alternative to graphene as a thin film transistor [73, 74], and as a photocatalytic agent [83]. It also highlights the differences that can occurs in TMDs between the bulk and thin films. Bulk MoS_2 is an indirect band gap semiconductor, but as it becomes a monolayer, its band gap becomes direct [73].

Applications for these materials are so varied because of the variety of phenomena in the TMDs themselves. $TiSe_2$ stands out as one of the more interesting TMDs. It only forms one polytype, 1T-$TiSe_2$, but this does not make it simple. While most TMDs exhibit ICDW behavior at high temperatures, a CCDW upon further cooling, followed by superconductivity at very low temperatures, pure $TiSe_2$ only has a transition from its normal state to a CCDW, and shows no superconducting state [25]. Additionally, the nature of its normal state has long been debated between an indirect small gap semiconductor or semi-metal, due to its small gap ($\Delta \sim 20$ meV) [35, 84–88]. Finally, unlike most low dimensional CDW compounds, $TiSe_2$ shows no Fermi surface nesting, making the origin of its CDW state unclear, with the Jahn–Teller effect or excitonic insulator (section 3.2) [37, 38] put forth as likely explanations.

In what follows in this section, we will consider the interplay between different correlated electronic states in TMDs. Chemical tuning in the TMDs is particularly versatile as intercalation (metals, M, occupying empty sites in the van der Waals gaps to form M_yTX_2), substitutional doping ($T'_zT_{1-z}X_2$), and deficiencies ($TX_{2-\delta}$) are all viable doping parameters. Depending on the dopant, different chemical or structural modifications can result: increased inter-layer distances as large organic molecules are intercalated may yield nearly single layer effects in the bulk, charge transfer from the intercalants to the host lattice may enhance the inter-layer coupling and drive the systems towards more 3D states, or superlattices can form from intercalant ordering. The physical properties can also be tremendously varied, and competition between different ground states (magnetic, superconducting, etc) can be observed depending on whether the dopant is a magnetic (M = magnetic 3d or 4f ions) or non-magnetic ion (M, T′ = alkaline earth, non-magnetic 4d or 5d transition metal).

5.2.1. CDWs and SC in TMDs. In TMDs, the competition between CDW and SC remains an open question. SC is observed in many TMDs as the CDW is suppressed by doping, pressure, intercalation, or defects [39, 59, 60, 81, 89–91]. In these materials, the CDW can coexist with SC and the CDW transition ends up at the dome of SC phases [39, 59, 92]. Alternatively, the CDW phase can be completely separated from the SC phase [81].

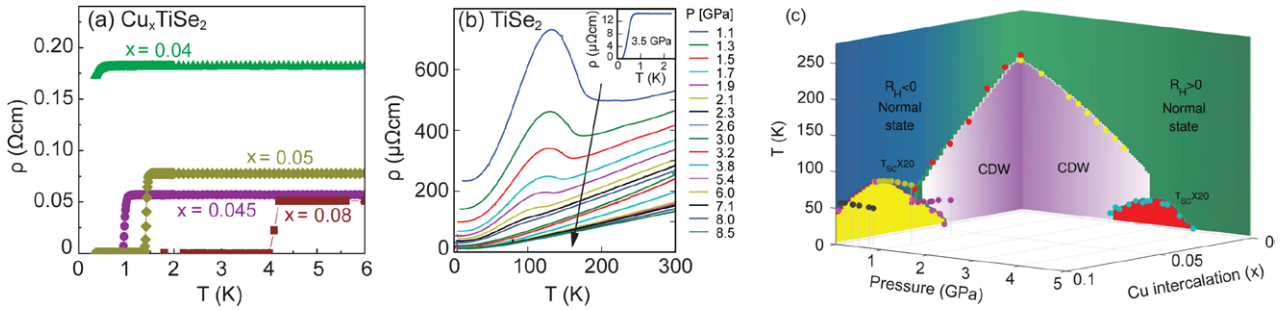

Figure 8. (a) Superconductivity induced by Cu-intercalation in 1T-$TiSe_2$ (reprinted with permission from [39], copyright 2006 Nature Publishing Group). (b) Superconductivity induced by pressure in 1T-$TiSe_2$ (reprinted with permission from [59], copyright 2009 APS). (c) Phase diagram of T_c, T_{CDW}, Cu intercalation, and pressure (reprinted with permission from [59], copyright 2009 APS).

The coexistence of CDW and SC indicates that these two electron order states are competing for the same electrons near the Fermi surface. However, there are systems (e.g. Pd_xTiSe_2 [81]) where the two phases are separated. The difference between these two scenarios points to the complexity of the underlying mechanisms of the formation of the CDW and SC states in these materials.

Many 2D TMDs TX_2 (T = Nb, Ta; X = S, Se, Te) have been intensively studied for their intrinsic CDW and SC states [28, 70, 93]. A CDW is observed in most of the TMDs but SC is only observed in a subset of these systems (mostly for T = Nb, Ta; X = S, Se) [28, 70, 93]. In stoichiometric TX_2, the CDW rarely coexists with SC except when the CDW is weakened by intercalation, pressure, or defects [39, 59, 60, 91, 92]. Most examples of the coexistence of CDW and SC are observed in the 1T polytype. This suggests that CDW and SC are more correlated in 1T than in 2H systems.

As discussed above, SC can be induced in TMDs by applying pressure or through chemical modifications. Defects in 1T-TaS_2 were reported to suppress the CDW and induce a SC transition. For TaS_2 single crystals, a CDW is observed in 1T-TaS_2, but no SC is observed down to $T = 0.4$ K. Li *et al* [60] showed that when defects were induced in single crystals of 1T-TaS_2 by quenching the crystals from high temperature, CDW order is suppressed and SC is enhanced and a SC transition appears at $T_C = 0.8$ K. Meanwhile, defects also enhance the SC transition temperature in 2H-TaS_2 from $T = 0.8$ K to 2.5 K.

Other than through defects, CDW in TMDs can be suppressed using doping, intercalation, and pressure. Meanwhile, SC appears and competes with CDW order. Liu *et al* [89] and Ang *et al* [90] showed that, although 1T-TaS_2 and 1T-$TaSe_2$ have CDW order with no SC down to $T = 0.4$ K, SC appears in 1T-$TaS_{2-x}Se_x$ within an intermediate doping range. SC also appears as the CDW in 1T-$TiSe_2$ is suppressed by intercalating Cu [39], Pd [81] or a misfit PbSe layer [94] (see section 5.2.3), with a SC dome stretching across a CDW QCP [95] or just outside the CDW state in the Cu and Pd cases, respectively. The comparison with Cu intercalation in 2H-TaS_2 [92] adds to the complexity of the interplay between SC and CDW in these TMDs. As mentioned above, 2H-TaS_2 already shows both CDW and SC, with critical temperatures around $T = 75$ K and 0.8 K respectively. In Cu_xTaS_2, T_C increases as T_{CDW} decreases, and the optimal SC state occurs around $x = 0.04$. While Cu intercalation may seem similar in the two compounds, it is remarkable that the optimal T_C values are very close, despite the face that the corresponding Cu compositions, x, differ by a factor of 2, and the critical fields ($H_c = 1.3$ T in the 1T-$TiSe_2$ and 4.9 T in 2H-TaS_2 compounds) are substantially different. Even more notable are the electronic considerations of Cu and Pd when intercalated in 1T-$TiSe_2$ [39, 81], where the former is believed to donate one electron to the TX_2 layer, with no electrons available in the latter. Add the fact that no other intercalant [96] has produced a SC state, and it is immediately apparent that a simple charge carrier picture does not account for the emergence of SC from the CDW state in these TMDs.

Furthermore, pressure is also demonstrated as a way to suppress CDW order and induce SC in 1T-$TiSe_2$ and 1T-TaS_2 [59, 91]. Using 1T-$TiSe_2$ as an example, the SC induced by Cu intercalation (figure 8(a)) and pressure (figure 8(b)) is summarized together with CDW transition in a phase diagram (figure 8(c)). All these examples show a competition between CDW and SC in TMDs.

5.2.2. Semi-metal to insulator transition and CDW suppression in $TiSe_2$. While the TMDs provide a rich playground for studying CDW and SC together, the CDW phenomenon can also be studied on its own. In this section, we will show remarkable chemical tuning of the electrical transport properties of $TiSe_2$ over nearly ten orders of magnitude. In the case of $TiSe_2$, the temperature profile of the synthesis has been found to have a drastic effect on the magnitude of the CDW transition [25]. This is due to the introduction of Se deficiency with increasing synthesis temperature, which results in a non-stoichiometry of the form $TiSe_{2-\delta}$. As seen in figure 9(a), a small amount of Se deficiency in $TiSe_2$ completely suppresses the CDW, resulting in metallic state down to the lowest measured temperatures. By contrast, doping Pt on the Ti site without Se deficiency, in $Ti_{1-z}Pt_zSe_2$, results in a large increase in the resistivity (nearly 8 orders of magnitude at low T for $z \leqslant 0.13$). Figure 9(a) shows the increasing resistivity with Pt concentration, and it appears that the CDW temperature remains unaffected by the doping, with only the CDW magnitude eventually concealed by the diverging resistivity in the insulating samples.

By tuning both the Se deficiency δ and the Pt substitution z at the same time in $Ti_{1-z}Pt_zSe_{2-\delta}$ (with $\delta = 2z$), a competition between the tendency towards metallicity (with increasing δ) and insulating behavior (with increasing z) ensues: the CDW gradually moves down in temperature, while the normal

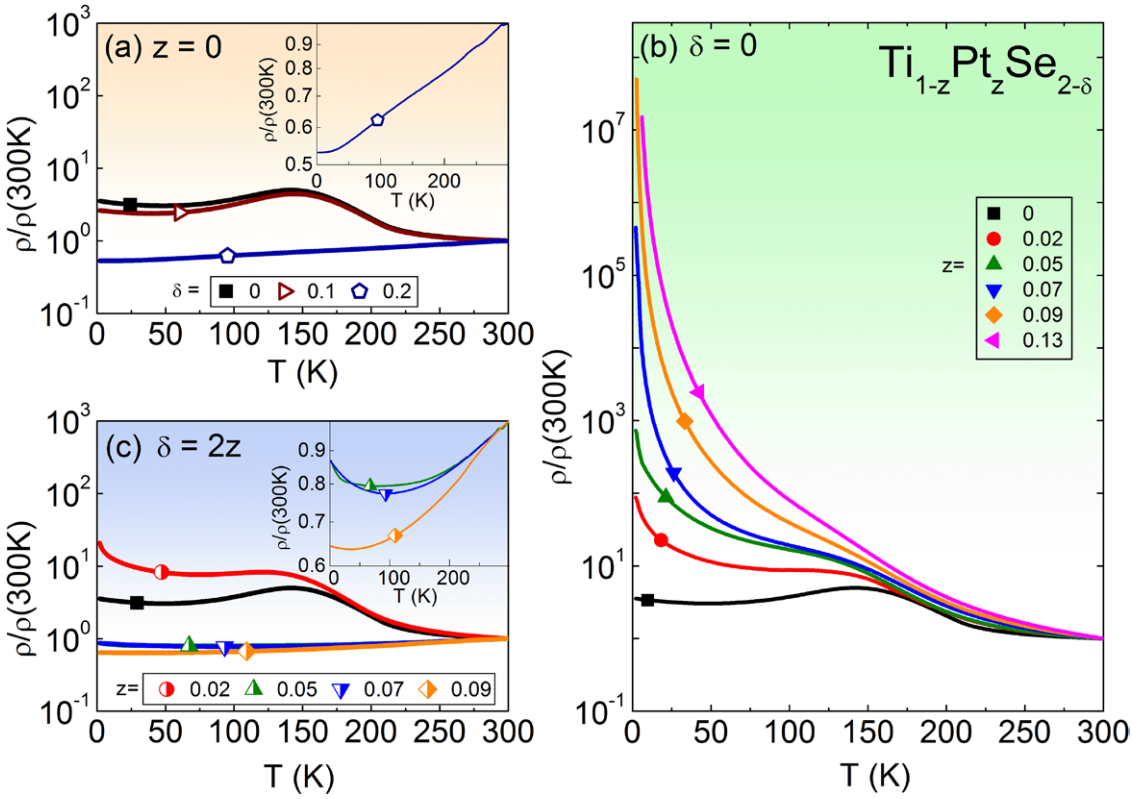

Figure 9. Resistivity plots for $Ti_{1-z}Pt_zSe_{2-\delta}$ with (a) Se deficiency, no Pt doping, (b) Pt doping, no Se deficiency, and (c) both Se deficiency and Pt doping (reproduced with permission from [97], copyright 2015 APS).

state becomes more and more metallic. Between the chemical parameters, almost 10 orders of magnitude in resistivity change at low temperature is registered in this system.

5.2.3. CDWs and magnetism in M_yTX_2 compounds. In their undoped state, most TMDs are paramagnetic or diamagnetic, though compounds often show Curie-Weiss behavior at low temperatures due to small amounts of magnetic impurities [98]. The majority of the magnetic behavior comes into play when TMDs are intercalated with a magnetic atom [99]. Unlike SC or the chalcogen deficiency where the CDW state is tunable, the introduction of a magnetic state dominates and conceals the CDW state. However, the unusual magnetic phenomena that arise are further indications of the complex interactions inherent in these systems. Similar to the non-magnetic systems, the properties of the M_yTX_2 systems depend not only on the choice of TMD and intercalant [99], but also on the amount of intercalant [99, 101]. As a result, these systems contain a wide breadth of phenomena from traditional FM and AFM order, to spin glass behavior [102], to mixed local and itinerant magnetic moment states [99]. We will focus on a few examples of the unusual magnetic behavior exhibited in these intercalated TMDs: the non-monotonic behavior in Fe_yTaS_2, sharp switching in the hysteresis curves of Fe_yTaX_2 (X = S, Se), and magnetoresistive behavior in WTe_2 and Fe_yTaS_2.

Non-monotonic behavior in Fe_yTaS_2. Fe_yTaS_2 showcases many of the unusual properties that arise with magnetic ion intercalation in the M_yTX_2 systems. As seen in figure 4(c), undoped 2H-TaS_2 exhibits a CDW at room temperature. Upon the intercalation of magnetic Fe, no CDW signatures are present, and the magnetic properties change in a non-monotonous manner as a function of the Fe content. The resulting Fe_yTaS_2 is FM for low Fe concentrations ($y < 0.4$), but becomes AFM at higher concentrations ($y > 0.4$) [101]. In addition, while still in the FM state, the Weiss temperature, θ_W, is non-monotonically dependent on the concentration y, as seen in table 1.

For the rational y values, $y = 1/4$ and $y = 1/3$, the Fe atoms form 2×2 and $\sqrt{3} \times \sqrt{3}$ superstructures respectively [104]. The $y = 1/4$ compound has the highest Curie temperature ($T_C = 160$ K), and it also exhibits a sharp magnetization switching [104]. The superstructure compositions also appear to have an drastic effect on the magnetoresistance of the samples.

Sharp magnetization switching in Fe_yTS_2 (T = Ta, Ti). In Fe_yTS_2 (T = Ta, Ti) systems, the $M(H)$ curves do not follow the traditional S-shaped hysteresis loop, but the magnetization switches direction abruptly at a critical field value H_s. The behavior is also reflected in sharp magnetoresistance drop at H_s. This is shown in figures 10(a)–(c) for $Fe_{0.25}TaS_2$ [104]. In Fe_yTiS_2, the magnetization switch, while sharp, is broader than in the Ta compound, and it occurs for a Fe composition close to $y = 2/3$ [105]. For both of these compounds, the sharp switching behavior occurs for specific iron concentrations. To date, these appear to be the only two intercalated TMDs to display such sharp magnetization switch with field. While the underlying mechanism for this effect remains largely understudied in the Ti compound, detailed studies of the

Table 1. Weiss temperature θ_W as a function of Fe content y in Fe_yTaS_2 (reproduced from [101, 103]).

Fe_yTaS_2									
y	0.20	0.25	0.26	0.28	0.30	0.33	0.34	0.40	0.45
θ_W (K)	90	135	165	90	91	70	55	10	−85

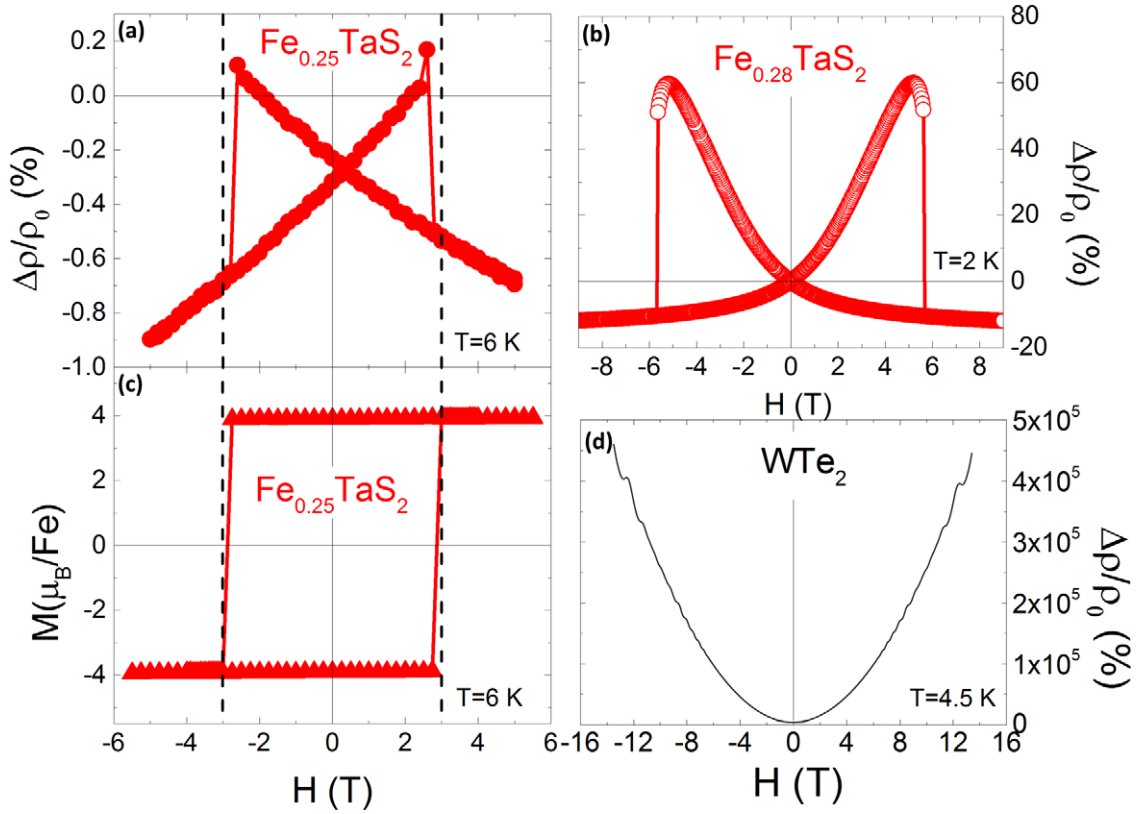

Figure 10. $\Delta\rho/\rho_0$ data for Fe_yTaS_2 for (a) $y = 0.25$ [104] and (b) $y = 0.28$ [108]. (c) $T = 2$ K $M(H)$ isotherm for $Fe_{0.25}TaS_2$. (d) $\Delta\rho/\rho_0$ data for WTe_2 (reproduced with permission from [79], copyright 2014 Nature Publishing Group).

magneto-transport properties in the Ta analogue have revealed remarkable behavior.

Large magnetoresistance in Fe_yTaS_2 and WTe_2. Magneto-optical studies on Fe_yTaS_2 ($y = 1/4$) have shown that the switching of magnetic domains occurs through the dendritic growth of one domain into another, suggesting strong c axis anisotropy as well as anisotropy with regards to the domain walls within the ab plane [106]. Magnetic susceptibility data in the radio frequencies suggest that the magnetic moment is local [106], which is further confirmed by ARPES and band structure calculations [107].

When the amount of Fe in Fe_yTaS_2 is changed slightly off the superstructure composition ($y = 0.28$), the magnetoresistance (figure 10(b)) displays a similar bow-tie shape to that for $y = 1/4$ (figure 10(a)). However, the absolute magnetoresistance value increases by nearly two orders of magnitude, from $\Delta\rho/\rho_0 \sim 1\%$ ($y = 0.25$) to $\sim 60\%$ ($y = 0.28$) [108]. These magnetoresistance values are comparable to the giant magnetoresistance values on thin film heterostructures where magnetic and non-magnetic layers are stacked analogous to the intercalation of magnetic atoms in between non-magnetic TX_2 layers. The drastic increase in magnetoresistance with a relatively small increase in iron concentration exemplifies the strong dependence of the TMD's magneto-transport properties on the crystal structure and the anisotropy. In Fe_yTaS_2, the magnetic moments act as Ising spins aligned along the c axis [104, 107]. When the moments are all aligned along an applied magnetic field H, for a critical switching field H_s some moments will flip anti-parallel to H. These anti-parallel spins act as carrier scatters, increasing resistivity. When Fe concentrations are away from the superstructures at $y = 1/4$ or 1/3, the intercalants or the superstructure vacancies act as defects which locally change the moment coupling strength [109]. In addition, the grain boundaries in the crystals can effectively pin the moments, effectively changing the overall magnetic properties [109].

A second notable example of a TMD system with unusual magneto-transport behavior is the semimetal WTe_2. WTe_2 does not fall into the 1T or 2H polytypes, but rather has an orthorhombic crystal structure. The tungsten forms chains along the a axis of the material, creating a quasi-1D structure within the quasi-2D structure. It exhibits magnetoresistance of a form similar to other semimetals like graphite and bismuth, with the resistance showing quadratic field dependence. However, it was recently reported that the magnetoresistance

of WTe_2 does not saturate up to 60 T [79], unlike graphite and bismuth which saturate at relatively low fields [110, 111]. With the applied field perpendicular to the *ab* plane, the magnetoresistance reaches up to 13,000,000% in fields up to 60 T. Figure 10(d) shows these data for fields up to 15 T. The system is highly anisotropic and, with the applied field parallel to the *ab* plane, the magnetoresistance is decreased by 90%.

The very large magnetoresistance is attributed to the effect of the semimetal's two band charge transport, with both *p* and *n* type carriers. This model predicts a resonance in the magnetoresistance when the *p* and *n* carriers are perfectly balanced (when $p/n \approx 1$). In graphite and Bi, slight deviances from $p/n = 1$ result in saturation at high fields [110, 111]. The small overlap between the bands in WTe_2 is similar to an excitonic insulator, which could mean that the balance between electrons and holes in this compound is close to perfect, preventing the magnetoresistance from saturating even at high fields [79].

Misfit structures in RX TX_2 (R = Sn, Pb, Sb, Bi, or rare earths). When trying to intercalate a TMD with certain dopants a misfit compound is formed instead. This consists of the TX_2 structure intermixed with a *RX* rocksalt structure. This is schematically shown in figure 7(b), where the intercalant layers are of the type RX. Since these two structures, RX and TX_2, have different symmetries and periodicities, long range order along the *c*-axis is not possible, thus making it an incommensurate or 'misfit' structure [94, 112]. As a result, these compounds tend to form with non-integer ratios between the numbers of RX and TX_2 layers. The dopants that form misfit layers are typically larger metals (R = Sn, Pb, Sb, Bi, or rare earths) [98, 113–115].

The intercalation of PbSe in the non-superconducting $TiSe_2$ results in a superconducting misfit compound [94]. There are strong parallels between this material and Cu_xTiSe_2 [39] as the intercalation results in the suppression of the CDW and a negative Seebeck coefficient throughout the range, indicating electron doping.

6. Summary

We have surveyed the mechanisms for the CDW formation in 1D systems and beyond, including the structural Peierls distortion, exciton formation, and the band Jahn–Teller mechanism. The focus is on the competition between various spin and electronic states, and in particular between CDWs and unconventional superconductivity or magnetism. We contrast the emergent phenomena caused by such competing states in two classes of compounds, the high temperature superconducting cuprates and the layered TMDs. In the former, magnetism is inherent to the parent compounds, and charge order (CDW states) has been known to exist mostly in the hole-doped cuprates. The strongest CDW occurs for hole content $p = 1/8$, for which the SC transition is suppressed almost completely in the '214' cuprates and only partially in the '123' systems. Together with a larger order parameter and a ~5 times larger correlation length in '214', this implies a better formed CDW than in '123'. More recent observations of CDW in the electron-doped '214' point to the asymmetrical behavior with electron- or hole-doping in cuprates. The correlation length in electron-doped '214' is nearly one order of magnitude smaller than in the hole equivalent case, with a CDW temperature T_{CDW} larger than that of the pseudogap T^* (T_{CDW} is comparable with T^* in the hole-doped case). Lastly, the complex Fermi surface and the nesting Fermi surface arcs observed in some cuprates ($Bi_2Sr_{2-x}La_xCuO_{6+\delta}$) point to possible correlations between the CDW and the pseudogap, yet to be fully understood.

The TMDs offer a rich field for tuning the existing CDW or SC states, or for inducing new ones via different chemical modifications. Doping, intercalation and defects present the possibility for chemical tuning in these layered materials, which in turn can result in strong intra-layer coupling and a 2D-to-3D crossover, or an increase in the layer spacing and a crossover in the opposite direction, towards true 2D behavior. Even small such perturbations have been observed to result in drastic changes in the electronic transport properties (e.g. $Pt_{1-z}Ti_zSe_{1-\delta}$), with the CDW almost unaffected by doping (finite *z*), or rapidly suppressed by defects (finite δ) (figure 9). CDW and SC exist in many TMDs, and extrinsic parameters such as doping or pressure have been employed to tune the balance between these two electronic states [92]. Remarkably, $TiSe_2$ is a TMD displaying a CDW transition and no SC, where intercalation of non-magnetic ions such as Cu or Pd results in the emergence of a SC dome, with the CDW suppressed at a QCP under the dome (in Cu_xTiSe_2, figure 8 [39]) or just outside the dome (in Pd_xTiSe_2 [81]). However, the temperature-composition phase diagrams are very similar in all intercalated superconducting TMDs, despite the different charge carrier concentrations contributed by the intercalants, or the different critical parameters (temperature or field). These observations are all testaments to the complexity of the superconductivity in the intercalated TMDs.

Unlike the cuprates, where magnetism is intrinsic to the parent compounds, the TMDs are non-magnetic, but intercalation with magnetic transition metals yields diverse magnetic order. This is best illustrated by the non-monotonous dependence of the magnetic order (AFM or FM) and the ordering temperature on the amount of Fe intercalated in 2H-TaS_2 [104, 108]. Remarkably sharp magnetization switching occurs in this system, especially when the magnetic ions form a superstructure as in 2H-$Fe_{0.25}TaS_2$ (figures 10(a) and (b)). Even more surprising, a small departure from the superstructure results in two orders of magnitude larger magnetoresistance in $Fe_{0.28}TaS_2$ (figure 10(c)). The only other TMD with comparably sharp magnetization switch is 2H-TiS_2 also intercalated with Fe. This raises the question of how does the 2H polytype lend itself to such anisotropy for the Fe^{2+} ions when intercalated in the Van der Waals gaps that favor the sharp switching of magnetic domains with magnetic field.

In lieu of conclusions, we offer these remarks as evidence for the complex phenomena associated with the electronic instabilities that result in CDW transitions. The body of work that we surveyed here attests to how unpredictable the electronic and magnetic states can be in strongly correlated

systems. Outstanding questions to be answered include: what role does the crystal structure and dimensionality play in the occurrence of CDW states in SCESs? how is the competition between electronic (SC, CDW) states resolved, and can it be understood in light of the Fermi surface topology, with or without Fermi surface nesting? are there correlations between CDW states and high temperature superconductivity? and how do magnetic order and CDW states interact? Understanding the CDW transitions themselves, and more importantly, addressing some of these questions will not only offer insights into the underlying physics of unconventional superconductivity but potentially make materials designed with targeted properties more predictable.

Acknowledgments

This work has been supported by the Gordon and Betty Moore Foundation's EPiQS Initiative through grant GBMF4417. The authors are grateful for fruitful discussions and input from B Rai, J Santiago, M Stavinoha, E Svanidze, and C Georgen.

References

[1] Hewson A C 1997 *The Kondo Problem to Heavy Fermions* vol 2 (Cambridge: Cambridge University Press)
[2] Bardeen J, Cooper L N and Schrieffer J R 1957 *Phys. Rev.* **108** 1175–204
[3] Thorne R E 1996 *Phys. Today* **49** 42
[4] Chan S K and Heine V 1973 *J. Phys. F: Met. Phys.* **3** 795
[5] Peierls R 1955 *Quantum Theory of Solids* (Oxford: Oxford University Press)
[6] Chaussy J, Haen P, Lasjaunias J C, Monceau P, Waysand G, Waintal A, Meerschaut A, Molinie P and Rouxel J 1976 *Solid State Commun.* **20** 759–63
[7] Grüner G 1988 *Rev. Mod. Phys.* **60** 1129–81
[8] Gressier P, Guemas L and Meerschaut A 1982 *Acta Crystallogr.* B **38** 2877–9
[9] Sato M, Fujishita H, Sato S and Hoshino S 1985 *J. Phys. C: Solid State Phys.* **18** 2603
[10] Krogmann K and Hausen H D 1968 *Z. Anorg. Allg. Chem.* **358** 67–81
[11] Renker B, Pintschovius L, Gläser W, Rietschel H, Comès R, Liebert L and Drexel W 1974 *Phys. Rev. Lett.* **32** 836–9
[12] Tranquada J M, Sternlieb B J, Axe J D, Nakamura Y and Uchida S 1995 *Nature* **375** 561–3
[13] Wu T, Mayaffre H, Kramer S, Horvatic M, Berthier C, Hardy W N, Liang R, Bonn D A and Julien M H 2011 *Nature* **477** 191–4
[14] Shin K Y, Laverock J, Wu Y Q, Condron C L, Toney M F, Dugdale S B, Kramer M J and Fisher I R 2008 *Phys. Rev.* B **77** 165101
[15] Leroux M, Rodiere P and Opagiste C 2013 *J. Supercond. Novel Magn.* **26** 1669–72 (arXiv:1301.2657)
[16] Galli F, Ramakrishnan S, Taniguchi T, Nieuwenhuys G J, Mydosh J A, Geupel S, Lüdecke J and van Smaalen S 2000 *Phys. Rev. Lett.* **85** 158–61
[17] Becker B, Patil N G, Ramakrishnan S, Menovsky A A, Nieuwenhuys G J, Mydosh J A, Kohgi M and Iwasa K 1999 *Phys. Rev.* B **59** 7266–9
[18] Singh Y, Pal D, Ramakrishnan S, Awasthi A M and Malik S K 2005 *Phys. Rev.* B **71** 045109
[19] Nagano Y, Araoka N, Mitsuda A, Yayama H, Wada H, Ichihara M, Isobe M and Ueda Y 2013 *J. Phys. Soc. Japan* **82** 064715
[20] Moore R G, Brouet V, He R, Lu D H, Ru N, Chu J H, Fisher I R and Shen Z X 2010 *Phys. Rev.* B **81** 073102
[21] Goh S, Tompsett D, Saines P, Chang H, Matsumoto T, Imai M, Yoshimura K and Grosche F 2015 *Phys. Rev. Lett.* **114** 097002
[22] Klintberg L E, Goh S K, Alireza P L, Saines P J, Tompsett D A, Logg P W, Yang J, Chen B, Yoshimura K and Grosche F M 2012 *Phys. Rev. Lett.* **109** 237008
[23] Grüner G 1994 *Density Waves in Solids* (Cambridge, MA: Addison-Wesley)
[24] He H and Zhang D 1999 *Phys. Rev. Lett.* **82** 811–4
[25] Di Salvo F J, Moncton D E and Waszczak J V 1976 *Phys. Rev.* B **14** 4321–8
[26] Comin R *et al* 2014 *Science* **343** 390–2
[27] Gabovich A M, Voitenko A I, Annett J F and Ausloos M 2001 *Supercond. Sci. Technol.* **14** R1
[28] Wilson J and Yoffe A 1969 *Adv. Phys.* **18** 193–335
[29] Wilson J A, Salvo F J D and Mahajan S 1975 *Adv. Phys.* **24** 117–201
[30] Steglich F, Aarts J, Bredl C D, Lieke W, Meschede D, Franz W and Schäfer H 1979 *Phys. Rev. Lett.* **43** 1892–6
[31] Bednorz J and Müller K 1986 *Z. Phys. B: Condens. Matter* **64** 189–93
[32] Kamihara Y, Watanabe T, Hirano M and Hosono H 2008 *J. Am. Chem. Soc.* **130** 3296–7
[33] Zhu X, Cao Y, Zhang J, Plummer E W and Guo J 2015 *Proc. Natl Acad. Sci.* **112** 2367–71
[34] Eiter H M, Lavagnini M, Hackl R, Nowadnick E A, Kemper A F, Devereaux T P, Chu J H, Analytis J G, Fisher I R and Degiorgi L 2013 *Proc. Natl Acad. Sci.* **110** 64–9
[35] Kidd T E, Miller T, Chou M Y and Chiang T C 2002 *Phys. Rev. Lett.* **88** 226402
[36] Jérome D, Rice T M and Kohn W 1967 *Phys. Rev.* **158** 462–75
[37] Rossnagel K, Kipp L and Skibowski M 2002 *Phys. Rev.* B **65** 235101
[38] Hughes H P 1977 *J. Phys. C: Solid State Phys.* **10** L319
[39] Morosan E, Zandbergen H W, Dennis B S, Bos J W G, Onose Y, Klimczuk T, Ramirez A P, Ong N P and Cava R J 2006 *Nat. Phys.* **2** 544–50
[40] Caprara S, Di Castro C, Grilli M and Suppa D 2005 *Phys. Rev. Lett.* **95** 117004
[41] Dordevic S V, Basov D N, Dynes R C and Bucher E 2001 *Phys. Rev.* B **64** 161103
[42] Chen C J 2008 *Introduction to Scanning Tunneling Microscopy* (Oxford: Oxford University Press)
[43] Hüfner S 2013 *Photoelectron Spectroscopy: Principles and Applications* vol 82 (Berlin: Springer)
[44] Inosov D S, Zabolotnyy V B, Evtushinsky D V, Kordyuk A A, Büchner B, Follath R, Berger H and Borisenko S V 2008 *New J. Phys.* **10** 125027
[45] Van Maaren M H and Schaeffer G M 1966 *Phys. Lett.* **20** 131
[46] Wise W D, Boyer M C, Chatterjee K, Kondo T, Takeuchi T, Ikuta H, Wang Y and Hudson E W 2008 *Nat. Phys.* **4** 696–9
[47] Arguello C J *et al* 2014 *Phys. Rev.* B **89** 235115
[48] Slough C G, McNairy W W, Coleman R V, Garnaes J, Prater C B and Hansma P K 1990 *Phys. Rev.* B **42** 9255–8
[49] Blume M 1985 *J. Appl. Phys.* **57** 3615–3618
[50] Hannon J P, Trammell G T, Blume M and Gibbs D 1988 *Phys. Rev. Lett.* **61** 1245–8
[51] Ghiringhelli G *et al* 2012 *Science* **337** 821–825
[52] Blanco-Canosa S *et al* 2013 *Phys. Rev. Lett.* **110** 187001
[53] Thampy V *et al* 2013 *Phys. Rev.* B **88** 024505
[54] Ament L J P, van Veenendaal M, Devereaux T P, Hill J P and van den Brink J 2011 *Rev. Mod. Phys.* **83** 705–67
[55] Wakimoto S *et al* 2009 *Phys. Rev. Lett.* **102** 157001
[56] Overhauser A W 1971 *Phys. Rev.* B **3** 3173–82
[57] Moncton D E, Axe J D and DiSalvo F J 1975 *Phys. Rev. Lett.* **34** 734–7

[58] Choe J, Morosan E and Kelly K Stm of fe_xtas_2 unsubmitted
[59] Kusmartseva A F, Sipos B, Berger H, Forró L and Tutiš E 2009 *Phys. Rev. Lett.* **103** 236401
[60] Li L J, Lu W J, Liu Y, Qu Z, Ling L S and Sun Y P 2013 *Phys. C: Supercond.* **492** 64–7
[61] Monthoux P, Pines D and Lonzarich G G 2007 *Nature* **450** 1177–83
[62] Hücker M *et al* 2014 *Phys. Rev.* B **90** 054514
[63] Fradkin E, Kivelson S A and Tranquada J M 2015 *Rev. Mod. Phys.* **87** 457–82
[64] Chang J *et al* 2012 *Nat. Phys.* **8** 871–6
[65] Blackburn E *et al* 2013 *Phys. Rev. Lett.* **110** 137004
[66] Bakr M *et al* 2013 *Phys. Rev.* B **88** 214517
[67] da Silva Neto E H, Comin R, He F, Sutarto R, Jiang Y, Greene R L, Sawatzky G A and Damascelli A 2015 *Science* **347** 282–285
[68] Perali A, Castellani C, Di Castro C and Grilli M 1996 *Phys. Rev.* B **54** 16216–25
[69] Castellani C, Di Castro C and Grilli M 1995 *Phys. Rev. Lett.* **75** 4650–3
[70] Chhowalla M, Shin H S, Eda G, Li L J, Loh K P and Zhang H 2013 *Nat. Chem.* **5** 263–75
[71] Kim Y, Huang J L and Lieber C M 1991 *Appl. Phys. Lett.* **59** 3404–6
[72] Tributsch H 1977 *Ber. Bunsenges. Phys. Chem.* **81** 361–9
[73] Mak K F, Lee C, Hone J, Shan J and Heinz T F 2010 *Phys. Rev. Lett.* **105** 136805
[74] Radisavljevic B, Radenovic A, Brivio J, Giacometti V and Kis A 2011 *Nat. Nanotechnol.* **6** 147–50
[75] Kyle J R, Ozkan C S and Ozkan M 2012 *Nanoscale* **4** 3807–19
[76] Lee J, Ha T J, Li H, Parrish K N, Holt M, Dodabalapur A, Ruoff R S and Akinwande D 2013 *ACS Nano* **7** 7744–50
[77] Lieth R M A 1977 *Preparation and Crystal Growth of Materials with Layered Structures* (Berlin: Springer)
[78] Morosan E, Natelson D, Nevidomskyy A H and Si Q 2012 *Adv. Mater.* **24** 4896–923
[79] Ali M N *et al* 2014 *Nature* **514** 205–8
[80] Naito M and Tanaka S 1982 *J. Phys. Soc. Japan* **51** 219–27
[81] Morosan E, Wagner K E, Zhao L L, Hor Y, Williams A J, Tao J, Zhu Y and Cava R J 2010 *Phys. Rev.* B **81** 094524
[82] Brudnyi A I and Karmadonov A F 1975 *Wear* **33** 243–9
[83] Zong X, Yan H, Wu G, Ma G, Wen F, Wang L and Li C 2008 *J. Am. Chem. Soc.* **130** 7176–7
[84] Cercellier H *et al* 2007 *Phys. Rev. Lett.* **99** 146403
[85] Cazzaniga M, Cercellier H, Holzmann M, Monney C, Aebi P, Onida G and Olevano V 2012 *Phys. Rev.* B **85** 195111
[86] May M M, Brabetz C, Janowitz C and Manzke R 2011 *Phys. Rev. Lett.* **107** 176405
[87] Li G, Hu W Z, Qian D, Hsieh D, Hasan M Z, Morosan E, Cava R J and Wang N L 2007 *Phys. Rev. Lett.* **99** 027404
[88] Rasch J C E, Stemmler T, Müller B, Dudy L and Manzke R 2008 *Phys. Rev. Lett.* **101** 237602
[89] Liu Y, Ang R, Lu W J, Song W H, Li L J and Sun Y P 2013 *Appl. Phys. Lett.* **102** 192602
[90] Ang R, Miyata Y, Ieki E, Nakayama K, Sato T, Liu Y, Lu W J, Sun Y P and Takahashi T 2013 *Phys. Rev.* B **88** 115145
[91] Sipos B, Kusmartseva A F, Akrap A, Berger H, Forro L and Tutis E 2008 *Nat. Mater.* **7** 960–5
[92] Wagner K E *et al* 2008 *Phys. Rev.* B **78** 104520
[93] Wang Q H, Kalantar-Zadeh K, Kis A, Coleman J N and Strano M S 2012 *Nat. Nano* **7** 699–712
[94] Giang N, Xu Q, Hor Y S, Williams A J, Dutton S E, Zandbergen H W and Cava R J 2010 *Phys. Rev.* B **82** 024503
[95] Barath H, Kim M, Karpus J F, Cooper S L, Abbamonte P, Fradkin E, Morosan E and Cava R J 2008 *Phys. Rev. Lett.* **100** 106402
[96] Morosan E unpublished
[97] Chen J S, Wang J K, Carr S V, Vogel S C, Gourdon O, Dai P and Morosan E 2015 *Phys. Rev.* B **91** 045125
[98] Baranov N V, Gerasimov E G and Mushnikov N V 2012 *Phys. Met. Metallogr.* **112** 711–44
[99] Parkin S S P and Friend R H 1980 *Phil. Mag.* B **41** 65–93
[100] Parkin S S P and Friend R H 1980 *Phil. Mag.* B **41** 95–112
[101] Narita H, Ikuta H, Hinode H, Uchida T, Ohtani T and Wakihara M 1994 *J. Solid State Chem.* **108** 148–51
[102] Negishi H, Ōhara S, Koyano M, Inoue M, Sakakibara T and Goto T 1988 *J. Phys. Soc. Japan* **57** 4083–5
[103] Eibschütz M, Mahajan S, DiSalvo F J, Hull G W and Waszczak J V 1981 *J. Appl. Phys.* **52** 2098–100
[104] Morosan E, Zandbergen H W, Li L, Lee M, Checkelsky J G, Heinrich M, Siegrist T, Ong N P and Cava R J 2007 *Phys. Rev.* B **75** 104401
[105] Negishi H, Shoube A, Takahashi H, Ueda Y, Sasaki M and Inoue M 1987 *J. Magn. Magn. Mater.* **67** 179–86
[106] Vannette M D, Yeninas S, Morosan E, Cava R J and Prozorov R 2009 *Phys. Rev.* B **80** 024421
[107] Ko K T *et al* 2011 *Phys. Rev. Lett.* **107** 247201
[108] Hardy W J, Chen C W, Marcinkova A, Ji H, Sinova J, Natelson D and Morosan E 2015 *Phys. Rev.* B **91** 054426
[109] Chen C W and Morosan E Large magnetoresistance induced by crystallographic defects in fe_xtas_2 single crystals unsubmitted
[110] Fauque B, Vignolle B, Proust C, Issi J P and Behnia K 2009 *New J. Phys.* **11** 113012
[111] Kopelevich Y, Torres J H S, da Silva R R, Mrowka F, Kempa H and Esquinazi P 2003 *Phys. Rev. Lett.* **90** 156402
[112] Wiegers G A and Meerschaut A 1992 *J. Alloys Compd.* **178** 351–68
[113] Wiegers G A 1996 *Prog. Solid State Chem.* **24** 1–139
[114] Pena O, Rabu P and Meerschaut A 1991 *J. Phys.: Condens. Matter* **3** 9929
[115] Suzuki K, Enoki T and Imaeda K 1991 *Solid State Commun.* **78** 73–7
[116] Hodeau J L *et al* 1978 Charge-density waves in $NbSe_3$ at 145K: crystal structures, x-ray and electron diffraction studies *J. Phys. C: Solid State Phys.* **11** 4117